EPJ Web of Conferences **49**, 15016 (2013)
DOI: 10.1051/epjconf/20134915016

Search for Exotic mono-jet and mono-photon signatures with the ATLAS detector

Reyhaneh Rezvani[1,2, a]

[1] *ATLAS collaboration*
[2] *University of Toronto, Canada*

Abstract. Mono-jet and mono-photon signatures are final states in a variety of scenarios beyond the Standard Model, such as the Large Extra Dimension models, gauge-mediated SUSY breaking scenarios, and models with pair production of Weakly Interacting Massive Particles considered as dark matter candidates. The produced exotic particles do not interact with the detector, resulting in missing transverse energy. The results of searches, performed in the ATLAS experiment at the LHC, for new physics in final states with an energetic jet or photon and large missing transverse energy are presented. The mono-jet search is performed using both 4.6 fb^{-1} of 7 TeV and 10.5 fb^{-1} of 8 TeV data, while the mono-photon results correspond to 4.6 fb^{-1} of 7 TeV data.

1 Introduction

Event topologies with one high transverse momentum [1] p_{T} jet or photon and large missing transverse energy are important final states for searches for new phenomena beyond the Standard Model (BSM) at the LHC. The large missing transverse energy can be a signature of weakly interacting particles not yet discovered. In order to tag such events, the processes are required to be accompanied by jets or photons. The BSM scenarios resulting in such final states include supersymmetry [1–3], Large Extra Dimensions (LED) scenarios [4, 5], and a general model for production of dark-matter weakly interacting massive particles (WIMP) [6]. In case the experimental studies of mono-jet and mono-photon events are consistent with Standard Model expectations, constraints will be set on the production of light gravitinos in association with gluinos or scalar quarks in the gauge-mediated SUSY breaking GMSB SUSY scenarios, the Planck scale of the LED model of Arkani-Hamed, Dimopoulos, Dvali (ADD), and the suppression scale in the pair production of WIMPs.

2 Mono-jet Analysis

The ATLAS [11] mono-jet analysis has been performed with 4.6 fb^{-1} of 7 TeV data [7], and has been updated with 10.5 fb^{-1} of 8 TeV data [8]. In the following, event selections, background determination methods, and the results are presented.

2.1 Event Selection

All data passing detector quality requirements are considered for the analysis. Events are required to pass a trigger that selects events with missing transverse momentum $E_{\mathrm{T}}^{\mathrm{miss}}$ above 80 GeV. This trigger is more than 95% efficient for offline reconstructed $E_{\mathrm{T}}^{\mathrm{miss}}$ above 120 GeV, and its efficiency is determined using an unbiased data sample with muons in the final state. Events should further satisfy a set of offline pre-selection and kinematic criteria as follows :

– Events are required to have a reconstructed primary vertex.

– Events should have $E_{\mathrm{T}}^{\mathrm{miss}} > 120$ GeV and at least one jet with p_{T} above 120 GeV and $|\eta| < 2$. Events with more than two jets with p_{T} above 30 GeV and in the region $|\eta| < 4.5$ are rejected. Furthermore, a cut on the azimuthal separation between $E_{\mathrm{T}}^{\mathrm{miss}}$ and the second jet (if present) is required, in order to reduce the QCD multi-jet background contribution where the large $E_{\mathrm{T}}^{\mathrm{miss}}$ originates from the mis-measurement of a jet : $|\Delta\phi(E_{\mathrm{T}}^{\mathrm{miss}}, 2^{nd}\, jet)| > 0.5$.

– Events are required to have no identified electrons or muons.

Four signal regions are defined with increasing symmetric lower thresholds of 120, 220, 350, and 500 GeV on the leading jet p_{T} and $E_{\mathrm{T}}^{\mathrm{miss}}$, referred to as SR1 - SR4.

a. e-mail: reyhaneh.rezvani@cern.ch

1. ATLAS uses a right-handed coordinate system with its origin at the nominal interaction point (IP) in the centre of the detector and the z-axis along the beam pipe. The x-axis points from the IP to the centre of the LHC ring, and the y-axis points upward. Polar coordinates (r, ϕ) are used in the transverse (x,y)-plane, ϕ being the azimuthal angle around the beam pipe. The pseudorapidity is defined in terms of the polar angle θ as $\eta = -\ln\tan(\theta/2)$.

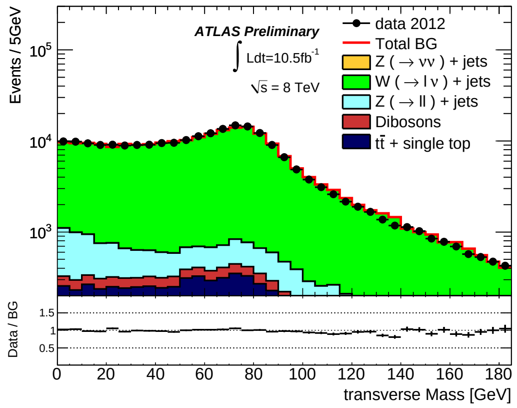

FIGURE 1. The measured transverse mass in the W($\mu\nu$)+jets control region, for the first signal region selection, compared to the background predictions. For illustration purposes, the ALPGEN W/Z+jet predictions from simulation are multiplied by a global scale factor 1.01 which brings the simulation predictions close to the data in the control region, allowing for a direct comparison of the shapes [8].

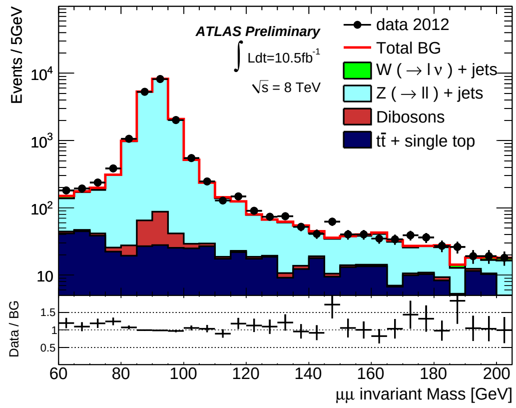

FIGURE 2. The measured di-muon invariant mass in the Z($\mu\mu$)+jets control region, for the first signal region selection, compared to the background predictions. For illustration purposes, the ALPGEN W/Z+jet predictions from simulation are multiplied by a global scale factor 0.97, which brings the simulation predictions close to the data in the control region, allowing for a direct comparison of the shapes [8].

2.2 Background Determination

The background to mono-jet events is dominated by Z ($\nu\nu$)+jets and W($\ell\nu$)+jets processes ($\ell = e, \mu, \tau$). It also includes contributions from Z/γ^*($\ell\ell$)+jets ($\ell = e, \mu, \tau$), QCD multi-jet, top, and diboson (WW,WZ, ZZ) processes. The W/Z+jets backgrounds, as well as the QCD multi-jet and non-collision backgrounds, are determined using data-driven techniques. Backgrounds from top and dibosons are determined using simulation samples.

Data control regions, orthogonal to the mono-jet signal regions, with identified electrons or muons in the final state and with the same requirements on the jets and $E_{\mathrm{T}}^{\mathrm{miss}}$, are defined to determine the W/Z+jets backgrounds. This reduces significantly the large theoretical and experimental systematic uncertainties associated with methods purely based on simulation.

The W($\mu\nu$)+jet data control regions are defined using muons with p_{T} above 7 GeV, and a transverse mass cut : 40 GeV $< m_{\mathrm{T}} <$ 100 GeV. The Z($\mu\mu$)+jets data control regions are defined requiring the presence of two oppositely charged muons with an invariant mass cut : 76 GeV $< m_{\mu\mu} <$ 116 GeV. The W($e\nu$)+jets data control regions are defined using an electron above 20 GeV in p_{T}. Figures 1 and 2 show the transverse mass and invariant mass distributions in the W($\mu\nu$)+jets and Z($\mu\mu$)+jets control regions.

To each data control region, simulation-based transfer factors are applied in order to get the background contribution in the mono-jet signal regions. As an example, the largest background Z($\nu\nu$)+jets in the signal region is determined from the W($\mu\nu$)+jets data control region according to :

$$N(\mathrm{Z}(\nu\nu){+}jets)_{signal} = (N^{data}_{control} - N^{background}_{control}) \times \frac{N^{MC}(\mathrm{Z}(\nu\nu) + jets)_{signal}}{N^{MC}(W(\mu\nu) + jets)_{control}}, \quad (1)$$

where $N^{MC}(\mathrm{Z}(\nu\nu) + jets)_{signal}$ is the background predicted by simulation in the signal region, and $N^{data}_{control}$, $N^{MC}(W(\mu\nu) + jets)_{control}$, and $N^{background}_{control}$ are the number of W($\mu\nu$)+jets candidates in data and simulation, and the non-electroweak background contribution in the control region, respectively. The latter refers to the top and diboson processes and is based on simulation. The transfer factor for each background process is defined as the ratio of simulated events for the process in the signal region over the total number of simulated events in the control region.

The contribution of QCD multi–jet events to mono-jet signal regions comes from those events for which the energy of a jet is badly measured such that the p_{T} of the jet falls below the 30 GeV jet definition threshold, therefore passing the signal selection cuts. Two types of data control regions are defined. For both types, all the signal selection cuts are applied except that the second jet above 30 GeV in p_{T} is required to be along the $E_{\mathrm{T}}^{\mathrm{miss}}$ direction in the first type $|\Delta\phi(E_{\mathrm{T}}^{miss}, 2^{nd}\,jet)| < 0.5$, and a third jet above 30 GeV in p_{T} is required along the $E_{\mathrm{T}}^{\mathrm{miss}}$ in the second type, $|\Delta\phi(E_{\mathrm{T}}^{\mathrm{miss}}, 3^{rd}\,jet)| < 0.5$. Extrapolation of the p_{T} distribution of these jets below the 30 GeV jet definition threshold gives an estimate of this background in the signal region.

2.3 Results

Good agreement is observed between data and the Standard Model predictions within the total background uncertainties, and model-independent 90% and 95% confidence level (CL) upper limits on the visible cross section, defined as the production cross section times acceptance times efficiency ($\sigma \times A \times \epsilon$), are set using the CL_s approach [9], as shown in Fig. 3 for the 8 TeV mono-jet analysis. Values of $\sigma \times A \times \epsilon$ above 2.8 pb, 0.16 pb, 0.05

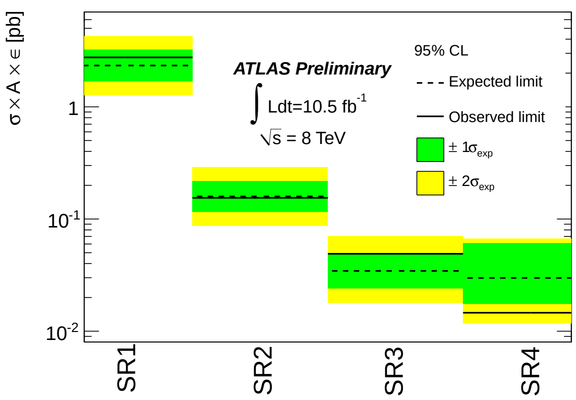

FIGURE 3. The model-independent observed (solid lines) and expected (dashed lines) 95% CL upper limits on $\sigma \times A \times \epsilon$ for different signal regions. The shaded areas around the expected limit indicate the $\pm 1\sigma$ and $\pm 2\sigma$ expected limits [8].

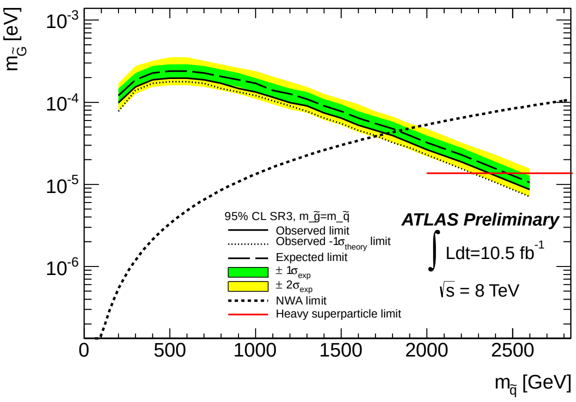

FIGURE 4. *[mono-jet analysis]* Observed (solid line) and expected (dashed line) 95% CL lower limits on the gravitino mass as a function of the squark mass for degenerate squark/gluino masses. The dotted line indicates the impact of the $\pm 1\sigma$ LO theoretical uncertainty on the observed limit. The shaded bands around the expected limit indicate the expected $\pm 1\sigma$ and $\pm 2\sigma$ expected limits. The dashed-dotted line defines the validity of the narrow-width approximation (NWA) used to obtain the decay rate of the gluino and squark to a gravitino and a parton. The solid red line denotes the current limit from LEP on the gravitino mass assuming very heavy squarks/gluinos [8].

pb, and 0.02 pb are excluded at 95% CL for the four defined signal regions, respectively.

The upper limits on the cross section can be translated to limits on a model parameter. Figures 4-6 show the resulting lower limits on the gravitino mass in the GMSB SUSY scenario for the degenerate case, the upper limits on the ADD signal yields as a function of the Planck scale M_D, and the lower limits on the WIMP suppression scale M^* for operator D5 of the effective theory used to calculate the cross sections. The lower limits on M^* can further be translated to upper limits on the WIMP-nucleon scattering cross section, as shown in Fig. 7 using the M^* limits of the 7 TeV mono-jet analysis.

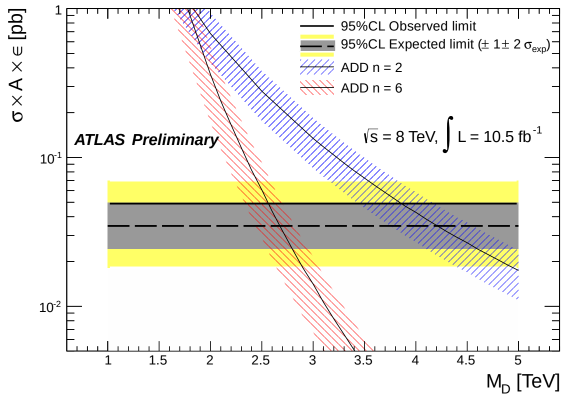

FIGURE 5. *[mono-jet analysis]* The predicted ADD $\sigma \times A \times \epsilon$ in the third signal region SR3 as a function of M_D for n=2 and n=6 extra spatial dimensions. The bands around the ADD curves show the effect of theoretical uncertainties. For comparison, the model-independent observed (solid line) and expected (dashed line) 95% CL upper limits on $\sigma \times A \times \epsilon$ are also shown. The shaded areas around the expected limit indicate the $\pm 1\sigma$ and $\pm 2\sigma$ expected limits [8].

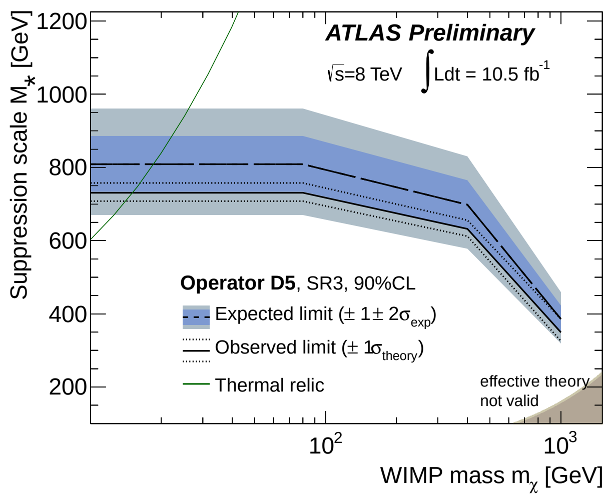

FIGURE 6. *[mono-jet analysis]* The 90% CL lower limits on M^* for different WIMP masses, for operator D5 of the effective theory. Observed and expected limits including all but the signal theoretical uncertainties are shown as dashed and solid black lines, respectively. The grey and blue bands around the expected limit are the $\pm 1\sigma$ and $\pm 2\sigma$ variations expected from statistical fluctuations and experimental systematic uncertainties on the Standard Model and signal processes. The impact of the theoretical uncertainties is shown by the thin black dotted $\pm 1\sigma$ limit lines around the observed limit. The M^* values at which WIMPs of a given mass would result in the required relic abundance are shown as the green line, assuming annihilation in the early universe proceeded exclusively via the given operator. The shaded light-grey region in the bottom right corner indicates where the effective field theory approach breaks down. The plot is based on the best expected limits, which corresponds to the third signal region SR3 in the 8 TeV mono-jet analysis [8].

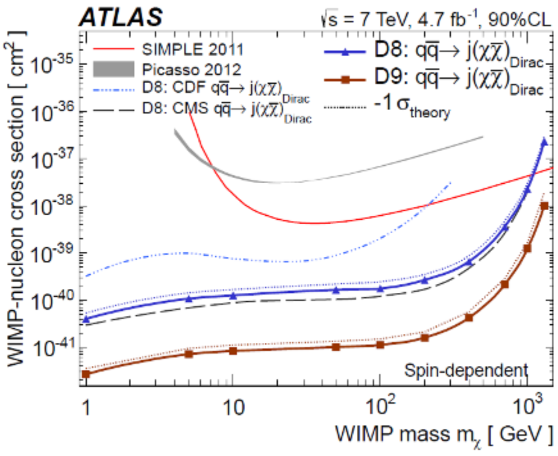

FIGURE 7. *[mono-jet analysis]* The 90% CL upper limits on spin-dependent WIMP-nucleon scattering cross sections versus WIMP mass. The thick solid lines are the observed limits excluding signal theoretical uncertainties. The dotted lines are the limits including the theoretical uncertainties. The ATLAS limits are for the four light flavours assuming equal coupling strengths for all quark flavours to the WIMPs. For comparison, 90% CL limits from the SIMPLE, Picasso, CDF, and CMS experiments are also shown [7].

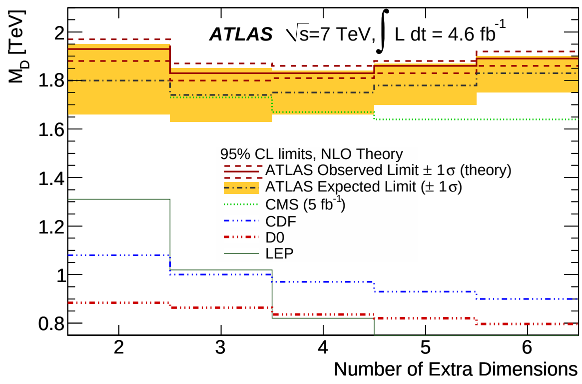

FIGURE 8. *[mono-photon analysis]* Observed (solid lines) and expected (dashed-dotted lines) 95% CL lower limits on the scale M_D as a function of the number of extra spatial dimensions n, in the ADD model [10].

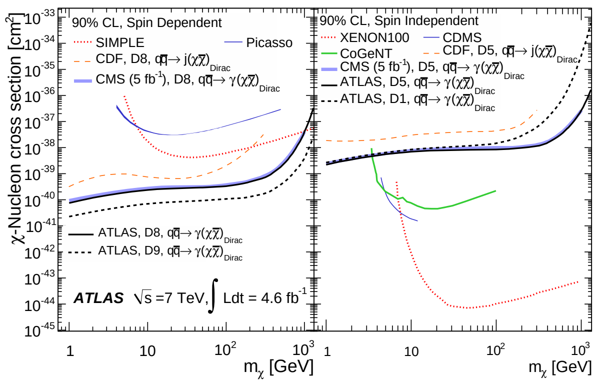

FIGURE 9. *[mono-photon analysis]* 90% CL upper limits on the WIMP-nucleon cross section as a function of the WIMP mass for spin-dependent [left] and spin-independent [right] interactions [10].

3 Mono-photon Analysis

The ATLAS mono-photon analysis has been performed with the 4.7 fb^{-1} 7 TeV data [10]. In the following, the event selections, background determination methods, and results are presented.

3.1 Event Selection

The data are collected using a trigger that selects events with $E_{\mathrm{T}}^{\mathrm{miss}}$ above 70 GeV. Events are further required to have $E_{\mathrm{T}}^{\mathrm{miss}}$ above 150 GeV. A photon is also required with $p_{\mathrm{T}} > 150$ GeV and $|\eta| < 2.37$, excluding the calorimeter barrel/end-cap transition regions ($1.37 < |\eta| < 1.52$). Events with more than one jet with $p_{\mathrm{T}} > 30$ GeV and $|\eta| < 4.5$ are rejected, while those with one such jet are kept in order to increase the signal acceptance and reduce systematic uncertainties related to the modelling of initial-state radiation. The reconstructed photon, $E_{\mathrm{T}}^{\mathrm{miss}}$, and jet (if present) are required to be well separated in the transverse plane with : $|\Delta\phi(E_{\mathrm{T}}^{\mathrm{miss}}, \gamma)| > 0.4$, $|\Delta\phi(E_{\mathrm{T}}^{\mathrm{miss}}, jet)| > 0.4$, and $|\Delta R(\gamma, jet)| > 0.4$. No identified electrons or muons should be present in the final state.

3.2 Background Determination

As in the mono-jet analysis, the background to mono-photon events is dominated by Z $(\nu\nu)+\gamma$. It also receives contributions from W/Z + γ events with unidentified electrons, muons or hadronic τ decays, and W/Z+jets events with an electron or a jet misreconstructed as a photon. In addition, there is a small contribution from top-quark, $\gamma\gamma$, diboson (WW,ZZ,WZ), γ+jets, and multi-jet processes. The same data-driven methods used in the mono-jet analysis are used to determine the electroweak, QCD multi-jet and γ+jet backgrounds. The background contributions from top-quark, $\gamma\gamma$, and diboson production processes are estimated using simulation samples. Non-collision background is estimated to be negligible.

3.3 Results

The data are found to be in good agreement with the Standard Model background-only hypothesis. The results are expressed in terms of model-independent 90% and 95% CL upper limits on the visible cross section, using the CL_s approach. Values of $\sigma \times A \times \epsilon$ above 5.6 fb and 6.8 fb are excluded at 90% CL and 95% CL, respectively. The results can further be translated to 95% CL lower limits on the scale M_D in the ADD scenario, and 90% CL upper limits on the WIMP-nucleon scattering cross sections, as shown in Fig. 8 and 9, respectively.

4 Conclusion

The ATLAS mono-jet and mono-photon analyses have been performed with the 7 and 8 TeV LHC pp collision data. Data-driven techniques have been used to determine the largest Standard Model backgrounds in both analyses. As good agreement has been observed between data and the expected Standard Model backgrounds, the results are interpreted as upper limits on the visible cross sections in various kinematic regions. These limits can further be used to constrain some BSM models that result in the mono-jet or mono-photon signatures, such as the ADD large extra dimensions scenario, the pair production of WIMP dark matter candidates, and the production of a gravitino in association with a squark/gluino, with the further decay of the squark/gluino to a gravitino and a parton, in GMSB scenarios.

References

[1] G. Giudice and R. Rattazzi, *Theories with gauge mediated supersymmetry breaking*, Phys.Rept. **322**, 419–499 (1999)

[2] P. Fayet, *Mixing Between Gravitational and Weak Interactions Through the Massive Gravitino*, Phys.Lett. **B70**, 461 (1977)

[3] R. Casalbuoni, S. De Curtis, D. Dominici, F. Feruglio, and R. Gatto, *A Gravitino-Goldstino High-Energy Equivalence Theorem*, Phys.Lett. **B215**, 313 (1988)

[4] N. Arkani-Hamed, S. Dimopoulos, and G. Dvali, *The Hierarchy problem and new dimensions at a millimeter*, Phys.Lett. **B429**, 263–272 (1998)

[5] G. F. Giudice, R. Rattazzi, and J. D. Wells, *Quantum gravity and extra dimensions at high-energy colliders*, Nucl.Phys. **B544**, 3-38 (1999)

[6] P. J. Fox, R. Harnik, J. Kopp, and Y. Tsai, *Missing Energy Signatures of Dark Matter at the LHC*, Phys.Rev. **D85**, (2012)

[7] ATLAS Collaboration, *Search for dark matter candidates and large extra dimensions in events with a jet and missing transverse momentum with the ATLAS detector*, arXiv :1210.4491 **[hep-ex]**, (2012)

[8] ATLAS Collaboration, *Search for New Phenomena in Monojet plus Missing Transverse Momentum Final States using 10 fb^{-1} of pp Collisions at $\sqrt{s}$ = 8 TeV with the ATLAS detector at the LHC*, ATLAS-CONF-2012-147, https://cdsweb.cern.ch/record/1493486 (2012)

[9] A. L. Read, *Presentation of search results : The CL_s technique*, J.Phys. **G28**, 2693–2704 (2002)

[10] ATLAS Collaboration, *Search for dark matter candidates and large extra dimensions in events with a photon and missing transverse momentum in pp collision data at $\sqrt{s}$ = 7 TeV with the ATLAS detector*, arXiv :1209.4625 **[hep-ex]**, (2012)

[11] ATLAS Collaboration, *The ATLAS Experiment at the CERN Large Hadron Collider*,JINST **3**, S08003 (2008)